Gene-Targeted Deletion of Neurofibromin Enhances the Expression of a Transient Outward K^+ Current in Schwann Cells: A Protein Kinase A-Mediated Mechanism

Yanfang Xu,[1,2,4] Nipavan Chiamvimonvat,[2] Ana E. Vázquez,[1] Shailaja Akunuru,[3] Nancy Ratner,[3] and Ebenezer N. Yamoah[1]

[1]Center for Neuroscience, Department of Otolaryngology, and [2]Department of Medicine, University of California, Davis, Davis, California 95616, [3]Department of Cell Biology, Neurobiology, and Anatomy, College of Medicine, University of Cincinnati, Cincinnati, Ohio 45267, and [4]Department of Pharmacology, Hebei Medical University, Shijiazhuang, Hebei 050091, China

Mutations in the neurofibromatosis type 1 gene predispose patients to develop benign peripheral nerve tumors (neurofibromas) containing Schwann cells (SCs). SCs from neurofibromatosis type-1 gene (*Nf1*) null mutant mice showed increased levels of Ras-GTP and cAMP. The proliferation and differentiation of SCs are regulated by Ras-GTP and cAMP-mediated signaling, which have been linked to expression of K^+ channels. We investigated the differential expression of K^+ currents in *Nf1* null mutant SCs (*Nf1*−/−) and their wild-type (*Nf1*+/+) counterparts and determined the mechanisms underlying the differences. The current densities of the sustained component of K^+ currents were similar in the two genotypes. However, *Nf1*−/− SCs showed a significant increase (~1.5-fold) in a 4-aminopyridine-sensitive transient outward K^+ current (I_A). Nonstationary fluctuation analysis revealed a significant increase in the number of functional channels in the null mutant cells. When the involvement of the Ras pathway in the modulation of the K^+ current was examined using adenoviral-mediated gene transfer of a dominant-negative H-Ras N17 or the known H-Ras inhibitor (L-739,749), an additional increase in I_A was observed. In contrast, protein kinase A (PKA) inhibitors, H89 and [PKI(2–22)amide] attenuated the enhancement of the current in the *Nf1*−/− cells, suggesting that the increase in I_A was mediated via activation of protein kinase A. The unitary conductance of the channel underlying I_A was unaltered by inhibitors of PKA. Activation of I_A is thus negatively regulated by Ras-GTP and positively regulated by PKA.

Key words: K^+ channels; protein kinase A; neurofibromin NF1; glia; Schwann cells; voltage clamp

Neurofibromatosis type 1 (NF1) is an inherited human autosomal disease, in which at least 95% of patients develop benign neurofibromas (Riccardi, 1991; Upadhyaya et al., 1992; Friedman and Birch, 1997; Cichowski and Jacks, 2001). The *NF1* gene, which is mutated in NF1 disease, encodes a GTPase activating protein (GAP) for Ras proteins called neurofibromin (Wallace et al., 1990; Xu et al., 1990). Schwann cells (SCs), which make up the majority of cells in neurofibromas, show increased levels of Ras-GTP, consistent with the loss of a negative Ras regulator (Kim et al., 1995). In addition, anti-Ras farnesyl protein transferase inhibitor partially restores the wild-type (WT) phenotype to *Nf1*-deficient mouse SCs (Kohl et al., 1995; Kim et al., 1997a). Non-Ras phenotypes of *Nf1*-mutant SC have also been characterized, but the molecular pathways underlying these phenotypes have not been identified (Kim et al., 1995, 1997b).

In contrast, the fruit fly (*Drosophila melanogaster*) *dNf1* null mutants show no obvious signs of perturbed Ras-mediated signaling; rather, these flies show involvement of the cAMP–protein kinase A (PKA) pathway (Guo et al., 1996, 1997; The et al., 1997; Tong et al., 2002). These defects result in loss of neuromuscular junction K^+ current activation in d*Nf1* mutants that can be rescued by elevation of cAMP (Guo et al., 1997; Tong et al., 2002). On the other hand, cells from NF1 patients with malignant peripheral nerve sheath tumors express enhanced K^+ currents; treatment of normal SCs with cAMP analogs confers the current phenotypes (Fieber, 1998). Thus, the regulation of ionic currents by the neurofibromin and/or its effectors may involve cAMP.

SCs from *Nf1* null mutant mice show a threefold elevation in the levels of cAMP compared with WT SCs (Kim et al., 2001). Thus, we hypothesized that SCs from *Nf1* null mutant mice might also have altered K^+ currents. In support of this line of investigation, damselfish infected with a virus develop neurofibroma-like tumors, with Schwann cells isolated from the tumors expressing enhanced K^+ currents compared with normal cells (Fieber and Schmale, 1994).

SC proliferation normally proceeds in parallel with increased expression of outward K^+ currents (Wilson and Chiu, 1993; Fieber, 1998; Kamleiter et al., 1998), and several SC growth-promoting factors, e.g., insulin-like growth factors, require cAMP (Stewart et al., 1991; Kim et al., 2001). Indeed, blockade of K^+ currents by quinine and tetraethylammonium chloride (TEA) impairs normal SC mitosis (Chiu and Wilson, 1989; Konishi, 1989a,b; Fieber, 1998; Sobko et al., 1998). Consistent with these notions, *Nf1* null mutant SCs show abnormal proliferation.

Here, we report that embryonic mouse SCs express a transient

Received May 7, 2002; revised Aug. 14, 2002; accepted Aug. 20, 2002.

This work was supported by National Institutes of Health Grants DC03828 and DC04215 (E.N.Y.), HL68507 and HL67737 (N.C.), and NS28804 (N.R.). We thank J. Nevins (Duke University, Durham, NC) for dnHa-Ras adenovirus, Mark Marchionni (Cambridge Neuroscience, Cambridge, UK) for glial growth factor, and Jackson Gibbs (Merck Research Labs, Somerset, NJ) for L739,749.

Correspondence should be addressed to Ebenezer N. Yamoah, Center for Neuroscience, Department of Otolaryngology, University of California, Davis, 1544 Newton Court, Davis, CA 95616. E-mail: enyamoah@ucdavis.edu.

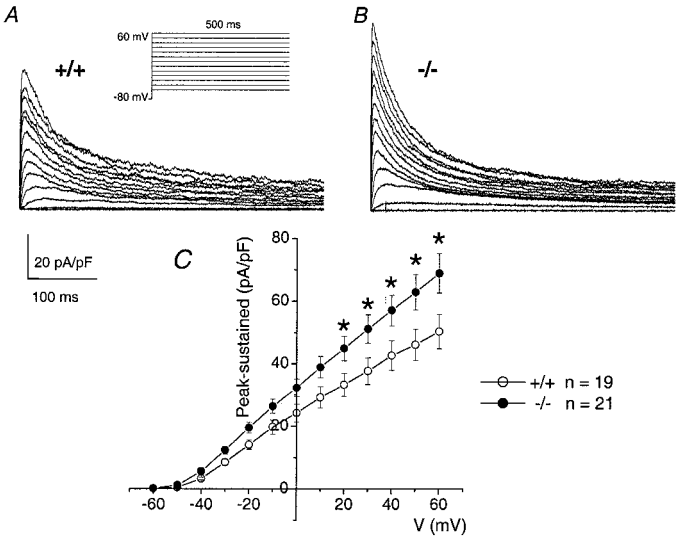

Figure 1. Enhanced current density of transient K^+ current in *NF1*−/− versus *Nf1*+/+ SCs. *A*, *B*, Examples of outward K^+ current traces recorded by using depolarizing voltage steps from a holding potential of −80 mV to step potential of 60 mV; data were obtained from SCs isolated from *Nf1*+/+ versus *Nf1*−/− mice, respectively. Shown in the *inset* is the voltage protocol used to elicit the current; duration of the voltage protocol was 500 msec. For comparison, the data are expressed as current density (picoamperes/picofarads). The mean capacitance (in picofarads) for *Nf1*+/+ and *Nf1*−/− Schwann cells were 15.1 ± 3.3 and 16 ± 4.5, respectively ($n = 25$; p = NS). *C*, The *I–V* relationships of the difference currents obtained by the subtraction of the sustained current densities from the peak current densities plotted as a function of voltage from *Nf1*+/+ (○) and *Nf1*−/− (●). The transient component of the outward K^+ current was significantly enhanced in the *Nf1*−/− Schwann cells at voltage steps positive to +20 mV (*$p < 0.05$). *n* represents the number of cells.

K^+ current blocked by 4-AP (I_A). More importantly, SCs isolated from *Nf1* null mutant mice showed an upregulation of this particular K^+ current. The increase in I_A was mediated via PKA by an increase in the number of functional channels. Activation of PKA pathway through K^+ channel activation may account for some Schwann cell phenotypes in neurofibromatosis type 1.

MATERIALS AND METHODS

Mouse SC culture. WT (*Nf1*+/+) and *Nf1* heterozygous mutant mice (*Nf1*+/−) in C57BL/6 background were derived and genotyped as described previously (Brannan et al., 1994). Because homozygous null mutant mice for *Nf1* die *in utero*, null mutant mouse embryos were obtained from the mating of *Nf1*+/− male and female mice. SCs were isolated from WT and *Nf1* null mutant mouse dorsal root ganglia (DRG) at embryonic day 12.5 before embryo death as described previously (Kim et al., 1995). Briefly, embryonic DRG were dissociated enzymatically, and cells from single embryos were plated onto six-well culture plates. DMEM supplemented with nerve growth factor (NGF) and human placental serum (10%) was used as culture medium. Culture medium was switched at day 2 in culture to N2 medium containing NGF and gentamycin (5 μg/ml). After 5–6 d in culture, SCs and neurons were separated from fibroblasts by lifting the SC neuron layers from the dish, leaving most of the fibroblasts attached to the culture dishes. Dissociated cells from the same genotype were pooled, and SCs were dissociated from the neurons using 0.01% collagenase. Cells were further centrifuged, resuspended in DMEM with 10% fetal bovine serum (FBS), and plated on poly-L-lysine-coated 100 mm cell culture plates at a density of $\sim 1 \times 10^6$ cells per plate. These cells were considered passage "0" (Kim et al., 1997a). Culture medium was switched the next day to SC growth media containing recombinant human glial growth factor 2 (10 ng/ml) (Cambridge Neuroscience, Norwood, MA) and 2 μM forskolin and 10% FBS. After 1 week in culture, cells were trypsinized and replated (passage "1"). The same step was further repeated once (passage "2") or twice (passage "3"). In all experiments, cells prepared between passage 1 and 3 were used because >99.5% of cells were SCs and are S100 positive and p75NGFR positive. SCs of designated genotype were plated near the center of poly-L-lysine-coated plastic 35 mm dishes, at ~100 cells per dish. Cells were then incubated in serum-free N2 medium for 48 hr before electrophysiological recordings.

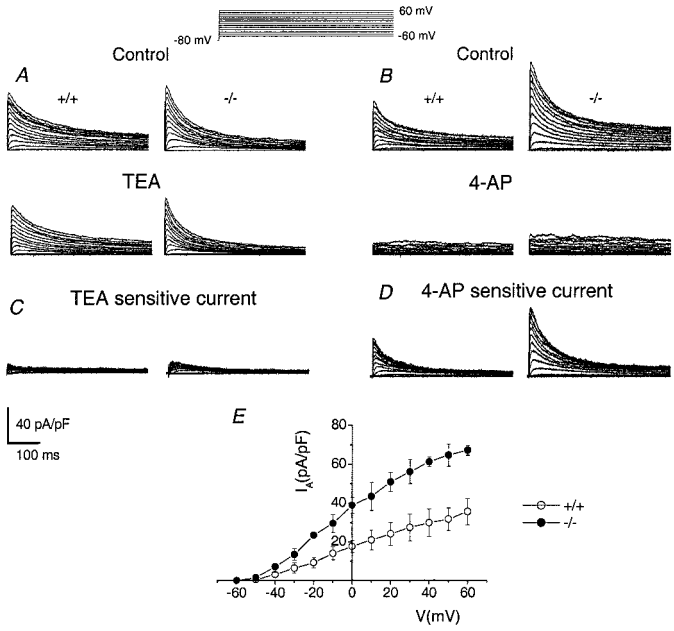

Figure 2. Effects of TEA and 4-AP on the transient outward current in Schwann cells. *A*, Current traces were generated using 500 msec depolarization pulses from a holding potential (V) of −80 mV to step potentials from −60 to 60 mV using a ΔV of 10 mV (see *inset*, voltage protocol) in the absence (*top panels*) and the presence (*bottom panels*) of 20 mM TEA-Cl in *Nf1*+/+ and *Nf1*−/− Schwann cells. *B*, Similar recordings were made in the absence and presence of 5 mM 4-AP. *C*, *D*, Here, we show the difference current traces, which represent the TEA-sensitive and 4-AP-sensitive currents, respectively. The predominant current is the 4-AP-sensitive component (I_A). Whereas TEA did not markedly alter the transient current in *Nf1*+/+ and *Nf1*−/− Schwann cells, 4-AP reduced the transient outward component of the current that was enhanced in *Nf1*−/− Schwann cells. *E*, The current density–voltage relationships of the 4-AP-sensitive component were derived from five cells from *Nf1*+/+ (○) and *Nf1*−/− (●) SCs.

Recombinant adenovirus containing dominant-negative Ras construct. Mouse SCs were plated in six-well plates coated with poly-L-lysine at 0.75×10^6 cells per well in DMEM with 0.5% FBS. After 24 hr in culture, cells were infected for 2 hr with recombinant adenovirus containing dominant-negative H-Ras N17 (DN-Ras) (gift from J. Nevins, Duke University, Durham, NC) in serum-free N2 medium (multiplicity of infection of 300). Media was changed to N2 for 48 hr after infection before electrophysiological experiments. Control cultures were infected with recombinant adenovirus expressing β-galactosidase at the same titers.

Electrophysiological recordings. Electrophysiological recordings were made 2–4 d after plating cells. Within this period, the size of SCs remained fairly constant with a mean cell capacitance of 15.6 ± 4.9 pF ($n = 69$). SCs were identified morphologically, i.e., cells with the characteristic bipolar spindle shape with long processes. Currents were recorded at room temperature using whole-cell and cell-attached configurations of the patch-clamp techniques (Hamill et al., 1981). For the cell-attached recordings, the tips of the pipettes were coated with Sylgard to reduce the pipette capacitance. Recordings were done using an Axopatch 200B patch-clamp amplifier (Axon Instruments, Foster City, CA) interfaced to a personal computer. Voltage commands were generated, and data were collected using custom-written software. During whole-cell recording, the capacitance of the cell was calculated by integrating the area under an uncompensated capacitive transient elicited by a 20 mV hyperpolarizing pulse from a holding potential of −40 mV. Cell capacitance and series resistance were then compensated as much as possible, almost to the point of ringing. In general, 60–80% of the series resis-

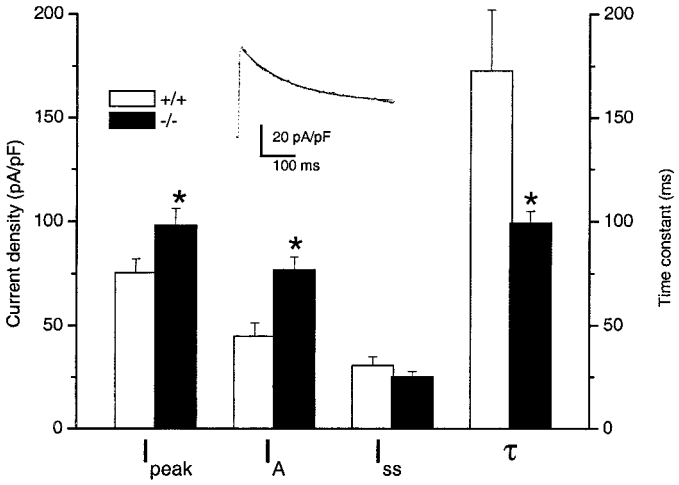

Figure 3. Analysis of the decay phase of the outward K^+ currents. The decay phases of the outward currents elicited from a holding potential of −80 mV to a test potential of +60 mV were fit using a single exponential function as described in Materials and Methods. The current decay (see *inset*) was well described by a single exponential, with decay time constants (τ) and a steady-state current (I_{SS} derived from A_{SS} of the exponential fit). The τ derived from these fits were significantly prolonged in the WT compared with mutant littermate cells ($^*p < 0.05$; $n = 11$). In addition, SCs derived from the mutant cells show an increase in the transient component (I_A derived from A_1 of the exponential fit) and total transient current (I_{peak}) compared with WT littermate cells.

tance was compensated. Current traces were amplified and filtered using an eight-pole Bessel filter at 2 kHz and digitized at 10 kHz. Currents were recorded using a holding potential of −80 mV and stepped to different depolarizing test pulses at frequencies between 0.2 and 0.5 Hz.

Chemicals and solutions. All chemicals were purchased from Sigma (St. Louis, MO) unless stated otherwise. For whole-cell recordings, the external solution contained the following (in mM): 140 *N*-methyl-D-glucamine, 5.4 KCl, 1 $MgCl_2$, 0.1 $CaCl_2$, 10 HEPES, and 10 glucose, pH 7.4 with methanesulfonic acid. Niflumic acid (50 μM) was added to the external solution to block Ca^{2+}-activated Cl^- currents. In some experiments, 4-AP and TEA were used. Pipette solution contained the following (in mM): 140 KCl, 4 Mg-ATP, 1 $MgCl_2$, 5 EGTA, and 10 HEPES, adjusted to pH 7.3 with KOH. For single-channel recordings, the bath solution consisted of the following (in mM): 145 KCl, 1 $MgCl_2$, 0.2 $CaCl_2$, 10 EGTA, and 10 HEPES, pH 7.4 with Tris buffer. Pipette solution was the same as the external solution used for whole-cell recordings. For experiments in which farnesyl transferase inhibitor (L-739,749) was used, cells were preincubated with 10 μM L-739,749 for 3–5 d in SC growth media before experiments. This dose of drug inhibits Ras processing in mouse SCs (Kohl et al., 1995; Kim et al. 1997b). The PKA inhibitors [PKI(2–22)amide] (PKI) and H89 were purchased from Calbiochem (La Jolla, CA) and were used at 5 μM, a concentration that effectively inhibits SC proliferation (Kim et al. 1997a).

Data analysis. Whole-cell K^+ current amplitudes at varying test potentials were measured at the peak and steady-state levels using a peak and steady-state detection routine. The current was normalized by the cell capacitance (in picofarads) to obtain the current density.

The decay phases of the transient outward currents evoked during a depolarizing voltage step to 60 mV from a holding potential of −80 mV were fitted by one exponential decay using the following expressions: $y(t) = A_1 * \exp(-t/\tau) + A_{ss}$, where t is time, τ is the time constant of decay of the inactivating K^+ currents, A_1 is the amplitude of the inactivating current components (I_A), and A_{ss} is the amplitude of the steady state, non-inactivating component of the total outward K^+ current (I_{SS}). Throughout this report, I_{peak} was used to describe the total peak current, which is determined using a peak detection routine in custom-written software. For all fits, time 0 was set at the peak of the outward current. For all analyses, correlation coefficients (R) were determined to assess the quality of fits, and R values for the fits reported here were ≥0.98.

Nonstationary fluctuation analysis was used to estimate the number (N) of functional channels in the membrane. For a homogeneous population of channels gating independently, the mean macroscopic current (I) is defined as follows: $I = N \cdot i \cdot P_o$. The macroscopic variance (σ^2) is defined as follows: $\sigma^2 = N \cdot i^2 \cdot P_o \cdot [1 - P_o]$, where i is the single-channel current amplitude, and P_o represents the open probability of the channel (Ehrenstein et al., 1970; Begenisich and Stevens 1975). The variance was calculated by subtracting pairs of sequential current records to obtain the difference current. The variance was then averaged over all of the records collected (Tsien et al., 1986). Provided that I and σ^2 are determined for a range of open probabilities, I and N can be estimated by a plot of variance versus mean current fit by the following parabolic function: $\sigma^2 = i \cdot I - I^2/N$ (Sigworth, 1977, 1980).

For single-channel records, leakage and capacitative transient currents were subtracted by fitting a smooth template to null traces. Leak-subtracted current recordings were idealized using a half-height criterion (Colquhoun and Sigworth, 1995). Transitions between closed and open levels were determined by using a threshold detection algorithm, which required that two data points exist above the half-mean amplitude of the single-unit opening. The computer-detected openings were confirmed by visual inspection, and sweeps with excessive noise were discarded. Amplitude histograms at a given test potential were generated and then fitted to a single Gaussian distribution using a Levenberg-Marquardt algorithm to obtain the mean and SD. At least five voltage steps and their corresponding single-channel currents were used to determine the unitary conductance. Single-channel current–voltage relationships were fitted by linear least-square regression lines, and single-channel conductances were obtained from the slope of the regression lines. Idealized records were used to construct ensemble-averaged currents and open probability. Curve fits and data analysis were performed using Origin software (Microcal Software, Northampton, MA). All averaged and normalized data are presented as means ± SD. The statistical significance of observed differences between groups of cells or between different parameters describing the properties of the currents were evaluated using a two-tailed Student's t test; p values are presented in the text, and statistical significance was set at $p < 0.05$.

RESULTS

Previous studies of WT SCs identified at least three outward K^+ currents (Fieber and Schmale, 1994). Fieber (1998) also showed that activation of protein kinase A enhances K^+ currents in human SCs. Examination of the effect of cAMP on mouse SCs confirmed the previous findings (data not shown). To determine whether K^+ currents are abnormal in *Nf1* null mutant SCs, we first identified the different components of K^+ currents in normal mouse SCs. K^+ currents were then recorded from *Nf1*−/− mouse SCs. To control for the possible variation between different batches of cells, K^+ currents were compared with WT and mutant cells obtained from embryonic littermates, at the same time point in culture.

Increased expression of a transient outward K^+ current in SCs isolated from *Nf1*−/− versus *Nf1*+/+ embryos

Figure 1 shows examples of outward K^+ currents recorded from *Nf1*+/+ SCs (*A*) compared with *Nf1*−/− SCs (*B*). Outward K^+ currents were elicited from a holding potential of −80 mV using step potentials from −60 to +60 mV in 10 mV increments. The outward K^+ currents were activated at step voltages positive to −50 mV. The currents were activated with a fast kinetics and inactivated rapidly to a sustained component. SCs from *Nf1*−/− null mutant mice show a significant upregulation of the transient outward K^+ current compared with cells isolated from the WT littermates. Summary data of the "difference current" obtained from subtraction of the peak and sustained components are shown in Figure 1*C*. Currents were normalized to the cell capacitance (in picofarads), and the sustained currents were measured as the currents at the end of the step potentials. At all test voltages more positive to +20 mV, the difference current (transient component) was enhanced significantly in *Nf1*−/− compared with *Nf1*+/+ ($^*p < 0.05$).

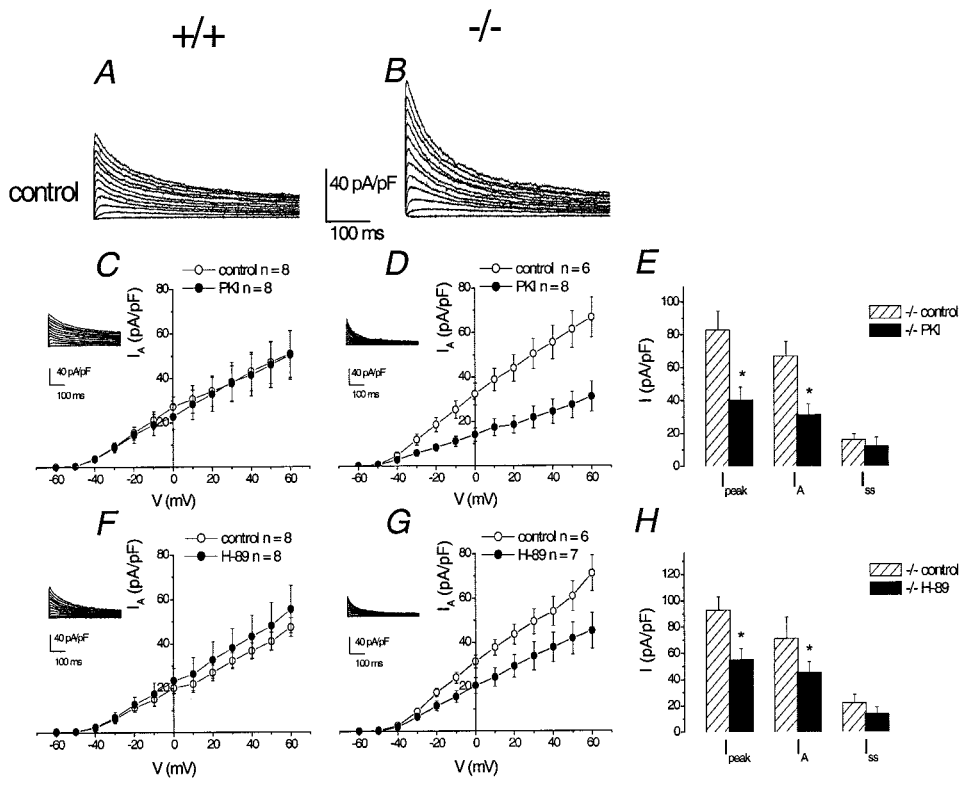

Figure 4. Effects of inhibitors of protein kinase A (PKI and H89) on I_A in *Nf1*+/+ versus *Nf1*−/− Schwann cells. *A*, *B*, Current traces were generated from *Nf1*+/+ and *Nf1*−/− SCs. The current traces were elicited using voltage protocols similar to the one described in Figure 2. *I–V* relationships of I_A from *Nf1*+/+ (*C*, *F*) and *Nf1*−/− (*D*, *G*) SCs recorded in the absence (○) or presence (●) of the PKA inhibitor (5 μM PKI or H89) in the pipette solution. PKI and H89 did not have substantial effect on the transient outward current (I_A) in *Nf1*+/+ SCs (*C*, *F*). In contrast, in the presence of PKI or H89 in the recording pipettes, the magnitude of the transient current in *Nf1*−/− SCs plummeted, as shown in the *I–V* relationships (*D*, *G*). The current traces shown as *insets* represent some of the raw data, after PKI–H89 application, that were used to generate the *I–V* relationships. *E*, *H*, Analyses of the decay kinetics of the outward K^+ currents, which were generated from a holding potential of −80 mV and stepped to a test potential of 60 mV from *Nf1*−/− confirmed a significant decrease of the I_{peak} and I_A by PKI or H89 ($^*p < 0.05$; $n = 6$). In contrast, the steady-state current (I_{SS}) was not significantly decreased in the presence of the PKA inhibitors [mean control I_{SS} (in picoamperes/picofarads) were 15.8 ± 3.5 and 22.2 ± 9.5; in the presence of PKI and H89, the mean I_{SS} were 12.0 ± 4.9 and 15.1 ± 9.1, respectively; in the presence of PKI, $n = 6$, $t_{(10)} = 1.57$, $p = 0.15$; in the presence of H89, $n = 6$, $t_{(10)} = 1.33$, $p = 0.21$].

To determine the identity of the outward K^+ current, TEA and 4-AP were applied to the bath solution to test for the presence of the transient and delayed rectifier K^+ currents (Konishi, 1989, 1990; Yamoah 1997; Fisher and Bourque, 1998). Figure 2, *A* and *B*, illustrates families of outward K^+ currents recorded from *Nf1*+/+ and *Nf1*−/− SCs in the absence and presence of the K^+ channel blockers. Based on the sensitivity toward 4-AP, at least two components of the outward K^+ currents can be identified: transient and sustained components. Whereas 4-AP blocked the transient outward current, TEA had no effect. Current traces representing the effects of 4-AP and TEA and the corresponding difference currents are shown in *C* and *D*. The 4-AP-sensitive current is the predominant K^+ current, and the summary data comparing the current density–voltage relationships between the WT and *Nf1*−/− SCs are depicted in Figure 2*E*. We tentatively classified the transient outward current as I_A based on its sensitivity toward 4-AP (Fieber and Schmale, 1994; Hille, 2001). These data confirmed our initial findings of the upregulation of the transient outward current described as the difference current in Figure 1*B*.

Additional analysis of the decay phases of the outward K^+ currents revealed that the current decay is well described by a single exponential, with decay time constant (τ) and a noninactivating (i.e., steady state) current (A_{SS}). The τ derived from these fits was prolonged in the WT compared with mutant littermates (Fig. 3).

Mechanisms for the enhancement of I_A in *Nf1*−/− SCs

Recent studies have demonstrated that the levels of cAMP is enhanced in mammalian *Nf1*−/− SCs (Kim et al., 2001), and activation of PKA has been implicated in SC proliferation (Kim et al., 1997a). In addition, SC proliferation has been linked to the expression of K^+ currents (Fieber, 1998). Therefore, we examined the effects of PKA inhibitors on I_A to determine whether activation of cAMP–PKA pathway may mediate the observed enhancement of the current in the null mutant cells. Two PKA inhibitors, PKI and H89, produced a substantial reduction of I_A in *Nf1*−/− SCs (Fig. 4*B*,*D*,*G*). In contrast, PKA inhibitors produced no observable effects on I_A density in the WT cells (Fig. 4*A*,*C*,*F*). Analysis of the decay kinetics was further performed as described previously on the mutant currents elicited at 60 mV. Both PKI and H89 resulted in a significant decrease in I_A in null mutant mice SCs (p *< 0.05; $n = 6$) (Fig. 4*E*,*H*), with no significant changes in the steady-state current [I_{SS}, $p = 0.15$ and 0.21 ($n = 6$) for the effects of PKI and H89, respectively].

Mutation of *Nf1* causes alterations in the cAMP–PKA pathway in Schwann cells. The Ras-GAP activity of neurofibromin is also important in *Nf1*-deficient mouse SCs. Indeed, anti-Ras farnesyl protein transferase inhibitor reversed several phenotypes of *Nf1*−/− SCs (Kohl et al., 1995; Kim et al., 1997a). To test the involvement of the Ras/GAP activity of neurofibromin in K^+ current modulation in SCs, we preincubated SCs with 10 μM L-739,749. This dose of the inhibitor was previously documented to inhibit H-Ras processing in mouse SCs (Kohl et al., 1995; Kim et al., 1997a). Figure 5*A* shows an enhancement of I_A density in SCs isolated from null mutant mice, after 3–5 d in culture with L-739–749. L-739,749 blocks farnesylation of proteins in addition to H-Ras. Therefore, to provide a definitive link between Ras and modulation of I_A, *Nf1*−/− SCs were infected with recombinant adenovirus containing DN-Ras. Recombinant adenovirus containing β-galactosidase was used as control. Consistent with results from L-739,749, adenoviral-mediated gene transfer of DN-Ras resulted in enhancement of I_A density in *Nf1*−/− SCs (Fig. 5*B*). No effects were observed in the WT littermates (data not shown; p = NS).

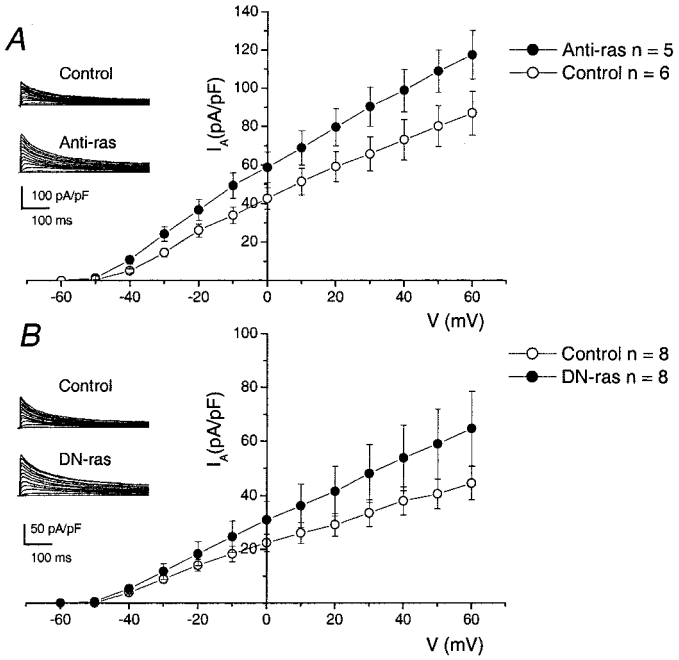

Figure 5. Enhancement of I_A density in *Nf1*−/− SCs by anti-Ras or DN-Ras. *A*, *I–V* relationships obtained from *Nf1*−/− SCs with (●) or without (○) pretreatment with anti-RAS (L-739,749). *B*, *I–V* relationships obtained from *Nf1*−/− SCs pretreated with recombinant adenovirus containing DN-Ras (●) versus β-galactosidase (○). The current traces shown as *inset* are examples of representative data that were used to generate the *I–V* relationship. Inhibition of Ras with L-739,749 or DN-Ras resulted in a significant increase in I_A density of traces elicited from potentials positive to 0 mV ($p < 0.05$) in *Nf1*−/− SCs. No effects were observed in the WT littermates (data not shown).

Single-channel properties of K^+ channels in *Nf1*+/+ and *Nf1*−/− SCs

The PKA-mediated enhancement of the macroscopic transient K^+ currents could stem from an increase in the microscopic currents, the number of functional channels, and a rise in the probability of channel openings (P_o), or a combination of these properties. To discriminate among these possibilities, single-channel currents were recorded using cell-attached patches in high K^+ external solution to depolarize the membrane potential to 0 mV. Figure 6*A* shows families of single-channel K^+ currents recorded from cell-attached patches from SCs isolated from WT compared with the *Nf1*−/− SCs. The ensemble-averaged currents were obtained from 200 consecutive sweeps of idealized single-channel records using a holding potential of −80 mV and a step potential of 50 mV, showing the transient nature of the current (Fig. 6*B*). In addition, the ensemble-averaged currents agreed well with the whole-cell data showing an increase in the inactivation kinetics in the null mutant mice compared with WT littermates. Amplitude histograms were constructed for the closed and open levels (Fig. 6*C*). The data indicate that, despite an increase in the whole-cell I_A density in the null mutant cells, there were no significant differences in the unitary current amplitudes obtained from the null mutant mice compared with WT littermates. Figure 6*D* shows unitary current–voltage relationships of I_A. There were no significant changes in the single-channel conductances (4.7 ± 1.0 vs 4.9 ± 1.3 pS for WT vs null mutant SCs, respectively; $n = 9$; $p = 0.67$; NS).

PKA modulate I_A by increasing the NP_o of the channel openings

Treatment of a cell-attached patch from *Nf1*−/− SCs containing I_A channel with H89 did not alter the unitary channel conductance but produced a profound decrease in the nP_o of the channel as shown in Figure 7. The mean conductance of the channel for control was 4.5 ± 0.5 pS and, after H89 treatment, was 4.6 ± 0.4 pS ($n = 5$; p = NS). In contrast, the nP_o decreased by approximately threefold compared with control values.

Nonstationary fluctuation analysis

As a direct means of estimating number of functional channels, we used nonstationary fluctuation analysis of whole-cell I_A using a test potential of 60 mV from a holding of −80 mV. Figure 8 shows plots of variance as a function of mean current in an SC isolated from WT (Fig. 8*A*) and null mutant (Fig. 8*B*) mice. The peak of the parabolic fit yields the number of functional channels, which is substantially higher in the null mutant than in the WT SCs. Recombinant adenovirus transfection of DN-Ras in SCs also enhanced the number of functional A-channels compared with β-galactosidase-transfected cells (Fig. 8*C*,*D*). Putting together data obtained from direct measurement of the macroscopic and microscopic channel activities show that PKA mediates an enhancement of the magnitude of a transient K^+ current by producing an increase in the nP_o of the channel most likely as a direct result of an increase in the number of functional channels (n).

In addition to the I_A described in Figure 6, a large conductance channel, with unitary current magnitude of ~5 pA at a step potential of 30 mV, was recorded from both *Nf1*+/+ and *Nf1*−/− SCs. Figure 9 illustrates families of single-channel traces recorded at different potentials. Ensemble-averaged current confirmed the sustained nature of the channel with unitary conductances of ~65 pS. Fig. 6*E* shows the open probability (nP_o) of the channels in the presence of H89. In contrast to I_A, the sustained current was insensitive to H89.

DISCUSSION

We defined the differences in K^+ current expression that exist between *Nf1*+/+ and *Nf1*−/− SCs from mouse dorsal root ganglia and have established the mechanisms underlying the differential expression. A transient K^+ current (I_A) is expressed in both *Nf1*+/+ and *Nf1*−/− SCs. However, I_A in the *Nf1*−/− SCs was significantly upregulated compared with the WT cells. The high level of expression of I_A in *Nf1*−/− SCs resulted from an increase in the nP_o of the channel, which is derived from an increase in the number of functional channels n. Although the precise function of I_A in Schwann cells is not known, its aberrant expression may have important implications for tumorigenesis in Schwann cells, because voltage-gated K^+ channel activity in glia is clearly linked to proliferation and differentiation (Chiu and Wilson, 1989; Gallo et al., 1996; Casaccia-Bonnefil et al., 1997; Knutson et al., 1997; Sobko et al., 1998).

Supporting a link between altered K^+ current alterations and SC tumorigenesis, SCs with mutations in the *NF2* tumor suppressor gene also have increased K^+ currents (Kamleiter et al., 1998; Rosenbaum et al., 2000), as do cells from malignant peripheral nerve sheath tumor cell (MPNST) lines (Fieber, 1998). Elevated transient outwardly rectifying K^+ currents also occur in damselfish neurofibroma SCs (Fieber and Schmale, 1994; Fieber, 1998). In the fish cells, neither the status of *NF1* gene mutations nor Ras-GTP or cAMP levels are known. MPNST cells have increased levels of Ras-GTP (Basu et al., 1992; DeClue et al., 1992)

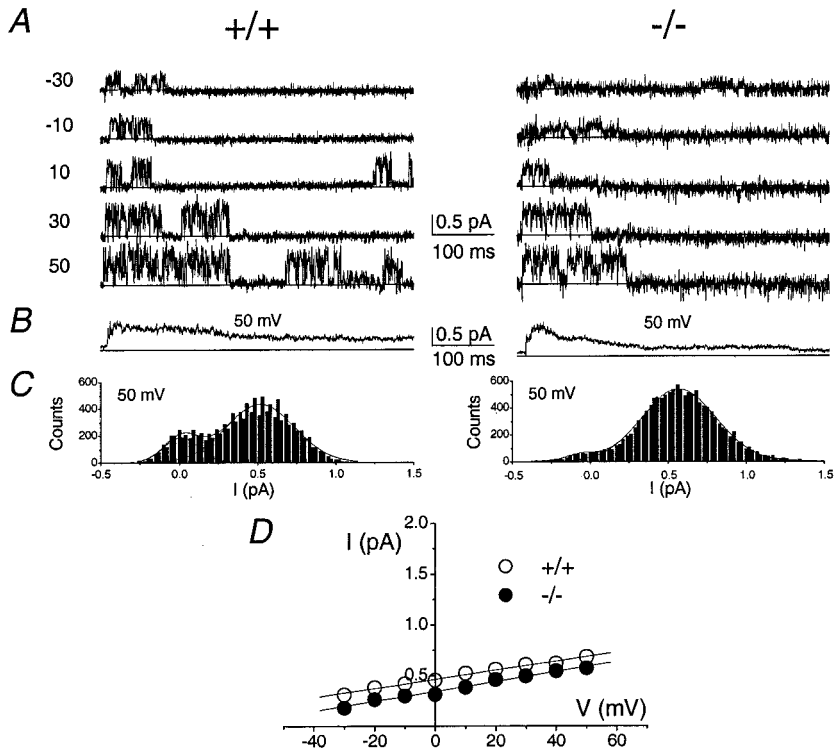

Figure 6. Single-channel currents recorded using cell-attached patches show no significant differences in the single-channel conductances in *Nf1*+/+ versus *Nf1*−/−. *A*, Families of single-channel K^+ currents recorded from cell-attached patches from SCs isolated from *Nf1*+/+ compared with *Nf1*−/− littermates from a holding potential of −80 mV. The voltage steps used are shown to the *left* of the current traces. Zero current levels are shown as *solid line*. *B*, Ensemble-averaged currents obtained from 200 consecutive sweeps of idealized single-channel records using a holding potential of −80 mV and a step potential of 50 mV showing the transient nature of the current. In addition, the ensemble-averaged currents show a rapid decay of the inactivation kinetics of the K^+ channel in *Nf1*−/− SCs compared with *Nf1*+/+ littermates. *C*, Amplitude histograms constructed for the closed and open levels. *D*, Unitary current–voltage relationships of I_A obtained from *Nf1*+/+ (○) compared with *Nf1*−/− (●). The single-channel conductances for the examples shown are 4.5 and 4.8 pS for WT versus null mutant cells, respectively. There was no significant difference between the conductance of the WT and mutant channels (in pS: WT, mean of 4.7 ± 1.0, $n = 9$; mutant, mean of 4.9 ± 1.3, $n = 9$; $t_{(16)} = 0.44$; $p = 0.67$).

and *NF1* mutations but also have numerous other genetic lesions that could contribute to the altered channel profile. In the mouse SC system in this report, we showed that primary SCs with *Nf1* gene mutations show increased K^+ currents. Our data suggest that *Nf1* mutation is directly linked to the phenotype of K^+ channel upregulation.

Nf1−/− SCs and activation of PKA result in an increase in the number of functional A-channels. Moreover, the data shown in the present study also suggest that the P_o of the channels may be altered. Although the whole-cell I_A was enhanced in the *Nf1*−/− SCs by ~1.5-fold compared with the WT cells, the functional number for channels were increased by approximately threefold, indicating that the P_o of the channels may be reduced in the *Nf1* mutant cells. We were unable to evaluate the exact effect of PKA activation–inhibition on the P_o of single A-channels because, for ~300 patches that were examined, none contained a single channel (one channel); the patches contained either no channel or had multiple channels. This may indicate that the A-channels are expressed in clusters. By altering the gating kinetics of inactivation of the A-channels, activation of PKA can potentially yield our present findings and thus masking and producing the apparent modest effect of PKI on the steady-state current (Fig. 4).

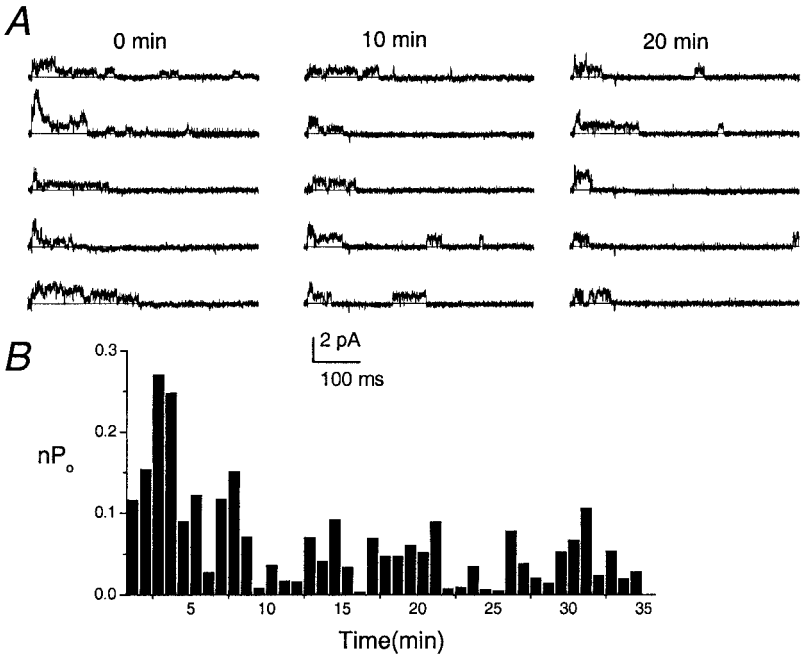

Figure 7. PKA modulates I_A by increasing the nP_o of channel openings. *A*, Cell-attached single-channel recordings of I_A from *Nf1*−/− SC using pipette containing H89. The single-channel traces were generated from a holding potential of −80 mV and stepped to a test potential of 0 mV, using a 500 msec pulse. Recordings were obtained at the beginning after giga-seal formation 0 min (*left*), 10 min (*middle*), and 20 min (*right*) into the recordings. Zero current levels (closed levels) are shown as *solid line*. H89 did not alter the unitary-channel conductance but produced a profound decrease in the nP_o of the channel. *B* shows a diary of the nP_o obtained at a test potential of 0 mV after formation of the seal. There was no significant difference between the conductance of the channel after H89 treatment (in pS: WT, control mean of 4.5 ± 0.5, $n = 5$; H89, mean of 4.6 ± 0.4, $n = 5$; $t_{(8)} = 0.51$; $p = 0.62$). However, nP_o decreased by approximately threefold in the presence of H89 compared with control values.

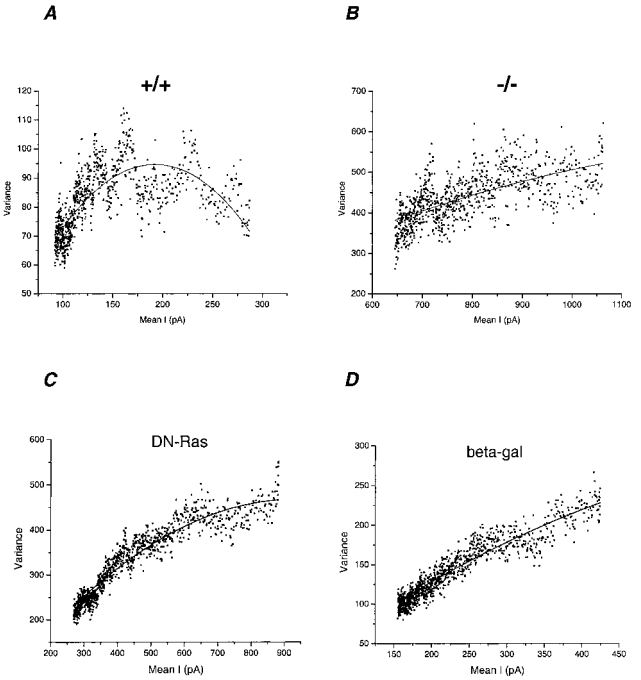

Figure 8. Nonstationary fluctuation analysis of I_A. The mean current at 60 mV is plotted versus variance for SCs from *Nf1*+/+ (*A*) and *Nf1*−/− (*B*). The cell capacitance for the examples shown are 9.0 and 9.6 pF for *Nf1*+/+ and *Nf1*−/−, respectively. Data from 200 consecutive current traces collected at 5 sec intervals are plotted. The *lines* represent best fits to the function $\sigma^2 = i \cdot I - (I^2/N)$, where σ^2, i, I, and N represent variance, single-channel current amplitude, macroscopic current, and total number of channels, respectively. With single-channel current amplitude of 0.75 (*Nf1*−/−) versus 0.98 pA (*Nf1*+/+), the number of channels was estimated to be 4.5 and 1.2 channels per square micrometer for the cells from *Nf1*−/− and *Nf1*+/+, respectively. *C*, *D*, Similar analyses were performed for DN-Ras and β-galactosidase control SCs. With single-channel current amplitude of 0.80 (DN-Ras) versus 0.82 pA [β-galactosidase (*beta-gal*)], the number of channels was estimated to be 3.7 and 1.8 channels per square micrometer for the DN-Ras and β-galactosidase control SCs, respectively.

Hence, detailed evaluation of the steady-state current in the presence of the I_A may be dependent on the duration of the pulse protocol. Finally, it is unlikely that the *Nf1*−/− SCs expressed a distinct subtype of K^+ channels because the single-channel conductances of the K^+ channels in the *Nf1*−/− and the WT SCs were similar. Rather, the functional number of channels and the gating phenotype of A-channels are altered in *Nf1*−/− SCs.

SCs from DRG and sciatic nerves of rats, rabbits, and mice express several 4-AP-sensitive transient outward K^+ currents (Chiu et al., 1984; Konishi, 1990; Amedee et al., 1991). None of the previously described currents is identical to I_A described here. However, the type 1 and type 2 currents defined by Pappas and Ritchie (1998) are each blocked by TEA and 4-AP, whereas the current we studied was blocked by 4-AP but was relatively insensitive to TEA. Other channel characteristics were similar to the type 1 channel in that it is a fast current activating at approximately −40 mV and showed sensitivity toward 4-AP.

K^+ α subunits are transmembrane proteins that assemble as tetramers to form K^+ selective pores (for review, see Nerbonne, 2000). The diversity of K^+ currents is increased by the interaction with auxiliary subunits and alternative splicing (for review, see Nerbonne, 2000). SCs express Kv1.1, Kv1.2, Kv1.4, Kv1.5, Kv2.1, Kv3.1, and Kv3.2 α subunits (Chiu et al., 1984; Pak et al., 1991; Mi et al., 1995). β2 subunits are not expressed in SCs (Rasband et al., 1998), but the status of other β subunits in SCs is not yet known. Peretz et al. (1999) suggested that a major SC I_A current is composed of the Kv1.4α subunits, as homomultimers and/or heteromultimers with Kv1.5 subunits. In heterologous systems, the heteromultimers generate a transient K^+ current with inactivation time constants (τ, ~40 msec) similar to a current in SCs (Po et al., 1993; Peretz et al., 1999). Whereas the inactivation time constant of the currents we observed differs slightly, inactivation of I_A current could be altered by developmental stage, species, and/or by the presence of specific β subunits or other auxiliary proteins in the channel complex.

In contrast to the differential expression of I_A, wild-type and *Nf1*−/− SCs expressed a sustained K^+ current at similar current

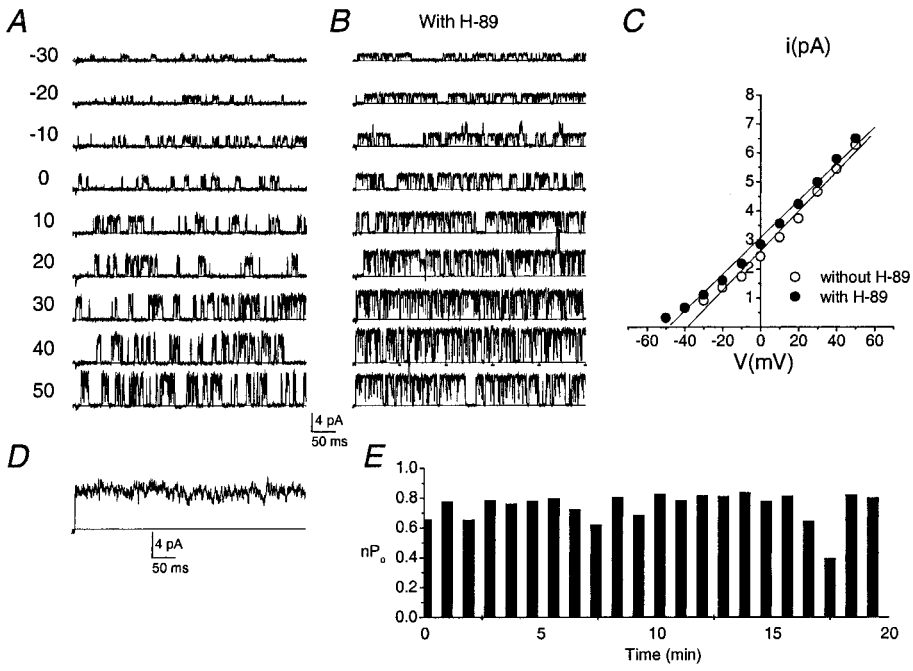

Figure 9. Single-channel recordings of sustained outward K^+ current. *A*, Families of single-channel current traces recorded from *Nf1*−/− using a holding potential of −80 mV. The test potential used are indicated to the *left* of the *traces*. *B*, Families of single-channel current traces recorded from *Nf1*−/− using a holding potential of −80 mV and the step potentials indicated; the pipette contained H89. *C*, Single-channel *I–V* relationships from the two different patches with or without H89. Similar unitary conductances were obtained. There was no significant difference between the conductance of the channel after H89 treatment (in pS: control mean of 65.1 ± 4.6, $n = 7$; H89, mean of 66.4 ± 8.6, $n = 7$; $t_{(12)} = 0.08$; $p = 0.94$). *D*, Ensemble-averaged current confirmed the sustained nature of the channel. *E*, The sustained current was insensitive to H89.

densities. The sustained K^+ current may be attributed to Kv1.5 or Kv1.1, which have been identified in SCs (Mi et al., 1995). This current is likely to correspond to the type 3 calcium-activated K^+ high conductance current identified by Howe and Ritchie (1988). Our data showed a slight decrease in the sustained component in the null mutant cells; however, the differences are not statistically significant. Alternatively, the apparent effect of PKA inhibitors on the sustained current may stem from the relatively short duration stimulus protocol (500 msec) used in the present study such that the I_{SS} measured was invariably masked by a residual I_A.

In *Nf1*−/− Schwann cells, elevated Ras-GTP, cAMP, or both might have caused altered channel properties. The *Nf1* gene product neurofibromin is a Ras/GAP (Xu et al., 1990), so that loss-of-function in *Nf1* equates to gain-of-function of Ras. In our experiments, inhibition of Ras-GTP with a dominant-negative Ras protein or a drug that blocks Ras activation by interfering with Ras translocation to the plasma membrane failed to block I_A. This strongly suggests that elevated Ras-GTP does not confer the mutant phenotype. Indeed, a small but significant potentiation of the I_A was observed with the Ras inhibitors.

In *Drosophila*, *Nf1* null mutations lead to downregulation of adenylate cyclase activity. Moreover, the *Nf1* null phenotype can be rescued by forskolin, an activator of adenylyl cyclase (Guo et al., 1996; The et al., 1997). In contrast, in mammalian SCs, loss-of-function of *Nf1* promotes, rather than inhibits, the formation of cAMP (Kim et al., 2001). How the loss of *Nf1* acts within Schwann cells to increase cAMP remains to be determined, but recent evidence suggests that neurofibromin regulates adenylyl cyclase(s) upstream of PKA (Tong et al., 2002). Strikingly, in our experiments, the inhibition of PKA by H89 or a PKA inhibitory peptide rapidly blocked the K^+ current. The use of PKI in the patch pipette allowed us to exclude the possibility that long-term changes driven by elevated cAMP affected channel density or function. In *Drosophila*, the K^+ channel altered in *dNf1* loss-of-function mutants requires both Ras-GTP and cAMP signaling to open in response to a neuropeptide (Zhong, 1995; Guo et al., 1997). In SCs, Ras-GTP and cAMP appear to antagonize channel opening. K^+ channel opening can be either increased or decreased by protein kinases, phosphatases, and cAMP (Ruby, 1988; Hoffman and Johnston, 1998). It is plausible that Ras-GTP, via downstream kinases or phosphatases, and PKA, directly or via cAMP, modulate phosphorylation of channel subunits and drive altered channel properties. Genistein, a broad-spectrum tyrosine kinase inhibitor, reduced the amplitude of a transient K^+ current (I_A) in mouse Schwann cell and affected its gating properties (Peretz et al., 1999). The Fyn tyrosine kinase increases delayed-rectifier K^+ channel activity in mouse Schwann cells, and exposure to tyrosine kinase inhibitors markedly downregulates voltage-gated K^+ (K_V) current amplitude and inhibits cell proliferation (Sobko et al., 1998a,b).

Schwann cells from *Nf1* knock-out mice have constantly high Ras-GTP and cAMP, but only cAMP drives channel activation. In wild-type cells, environmental factors, such as platelet-derived growth factor, basic fibroblast growth factor, insulin-like growth factor, and Reg-1, all transiently activate Ras-GTP and promote Schwann cell growth, but only when cAMP is high (Davis and Stroobant, 1990; Eccleston et al., 1990; Stewart et al., 1991; Jessen and Mirsky, 1992; Kim et al., 1997a,b, 2001; Livesey et al., 1997; Howe and McCarthy, 2000). Thus, the combination of tyrosine kinase signals and cAMP precisely regulate Schwann cell response to growth factors. The disrupted balance between Ras-GTP and cAMP in Nf1 mutant Schwann cells may, at least in part via K^+ current modulation, contribute to the hyperplastic growth exhibited by Nf1 null SCs or their precursors in serum-free medium (Kim et al., 1997a,b) and to the development of Schwann cell tumors in patients with type 1 neurofibromatosis.

REFERENCES

Amedee T, Ellie E, Dupouy B, Vincent JD (1991) Voltage-dependent calcium and potassium channels in Schwann cells cultured from dorsal root ganglia of the mouse. J Physiol (Lond) 441:35–56.

Basu TN, Gutmann DH, Fletcher JA, Glover TW, Collins FS, Downward J (1992) Aberrant regulation of ras proteins in malignant tumour cells from type 1 neurofibromatosis patients. Nature 356:713–715.

Begenisich T, Stevens CF (1975) How many conductance states do potassium channels have? Biophys J 15:843–846.

Brannan CI, Perkins AS, Vogel KS, Ratner N, Nordlund ML, Reid SW, Buchberg AM, Jenkins NA, Parada LF, Copeland NG (1994) Targeted disruption of the neurofibromatosis type-1 gene leads to developmental abnormalities in heart and various neural crest-derived tissues. Genes Dev 8:1019–1029.

Casaccia-Bonnefil P, Tikoo R, Kiyokawa H, Friedrich Jr V, Chao MV, Koff A (1997) Oligodendrocyte precursor differentiation is perturbed in the absence of the cyclin-dependent kinase inhibitor p27Kip1. Genes Dev 11:2335–2346.

Chiu SY, Wilson GF (1989) The role of potassium channels in Schwann cell proliferation in Wallerian degeneration of explant rabbit sciatic nerves. J Physiol (Lond) 408:199–222.

Chiu SY, Schrager P, Ritchie JM (1984) Neuronal-type Na^+ and K^+ channels in rabbit cultured Schwann cells. Nature 311:156–157.

Cichowski K, Jacks T (2001) NF1 tumor suppressor gene function: narrowing the GAP. Cell 104:593–604.

Colquhoun D, Sigworth F (1995) Fitting and statistical analysis of single-channel records. In: Single-channel recording, Ed 2 (Neher E, ed), pp 483–585. New York.: Plenum.

Davis JB, Stroobant P (1990) Platelet-derived growth factors and fibroblast growth factors are mitogens for rat Schwann cells. J Cell Biol 110:1353–1360.

DeClue JE, Papageorge AG, Fletcher JA, Diehl SR, Ratner N, Vass WC, Lowy DR (1992) Abnormal regulation of mammalian p21ras contributes to malignant tumor growth in von Recklinghausen (type 1) neurofibromatosis. Cell 69:265–273.

Eccleston PA, Collarini EJ, Mirsky R, Jessen KR, Richardson WD (1990) Platelet derived growth factor stimulates Schwann cell DNA synthesis. Neuroscience 2:985–992.

Ehrenstein G, Lecar H, Nossal R (1970) The nature of the negative resistance in bimolecular lipid membranes containing excitability-inducing material. J Gen Physiol 55:119–133.

Fieber LA (1998) Ionic currents in normal and neurofibromatosis type 1-affected human Schwann cells: induction of tumor cell K current in normal Schwann cells by cyclic AMP. J Neurosci Res 54:495–506.

Fieber LA, Schmale MC (1994) Differences in a K current in Schwann cells from normal and neurofibromatosis-infected damselfish. Glia 11:64–72.

Fisher TE, Bourque CW (1998) Properties of the transient K^+ current in acutely isolated supraoptic neurons from adult rat. Adv Exp Med Biol 449:97–106.

Friedman JM, Birch PH (1997) Type 1 neurofibromatosis: a descriptive analysis of the disorder in 1,728 patients. Am J Med Genet 70:138–143.

Gallo V, Zhou JM, McBain CJ, Wright P, Knutson PL, Armstrong RC (1996) Oligodendrocyte progenitor cell proliferation and lineage progression are regulated by glutamate receptor-mediated K^+ channel block. J Neurosci 16:2659–2670.

Guo F, The I, Bernards A, Hariharan I, Zhong Y (1996) Role of neurofibromin 1 in signal transduction mediating neuropeptide response. Soc Neurosci Abstr 22:375.

Guo F, The I, Hannan F, Bernards A, Zhong Y (1997) Requirement of *Drosophila* NF1 for activation of adenylyl cyclase by PACAP38-like neuropeptides. Science 276:795–798.

Hamill OP, Marty A, Neher E, Sakmann B, Sigworth FJ (1981) Improved patch-clamp techniques for high-resolution current recording from cells and cell-free membrane patches. Pflügers Arch 391:85–100.

Hille B (2001) Ion channels of excitable membranes, Ed 3. Sunderland, MA: Sinauer.

Hoffman AD, Johnston D (1998) Downregulation of transient K^+ channels in dendrites of hippocampal CA1 pyramidal neurons by activation of PKA and PKC. J Neurosci 18:3521–3528.

Howe DG, McCarthy KD (2000) Retroviral inhibition of cAMP-dependent protein kinase inhibits myelination but not Schwann cell mitosis stimulated by interaction with neurons. J Neurosci 20:3513–3521.

Howe JR, Ritchie JM (1988) Two types of potassium current in rabbit cultured Schwann cells. Proc R Soc Lond B Biol Sci 235:19–27.

Jessen KR, Mirsky R (1992) Schwann cells: early lineage, regulation of

proliferation and control of myelin formation. Curr Opin Neurobiol 2:575–581.
Kamleiter M, Hanemann CO, Kluwe L, Rosenbaum C, Wosch S, Mautner VF, Muller HW, Grafe P (1998) Voltage-dependent membrane currents of cultured human neurofibromatosis type 2 Schwann cells. Glia 24:313–322.
Kim HA, Rosenbaum T, Marchionni MA, Ratner N, DeClue JE (1995) Schwann cells from neurofibromin deficient mice exhibit activation of p21ras, inhibition of cell proliferation and morphological changes. Oncogene 11:325–335.
Kim HA, Ling B, Ratner N (1997a) Nf1-deficient mouse Schwann cells are angiogenic and invasive and can be induced to hyperproliferate: reversion of some phenotypes by an inhibitor of farnesyl protein transferase. Mol Cell Biol 17:862–872.
Kim HA, DeClue JE, Ratner N (1997b) cAMP-dependent protein kinase A is required for Schwann cell growth: interactions between the cAMP and neuregulin/tyrosine kinase pathways. J Neurosci Res 49:236–247.
Kim HA, Ratner N, Roberts TM, Stiles CD (2001) Schwann cell proliferative responses to cAMP and Nf1 are mediated by cyclin D1. J Neurosci 21:1110–1116.
Knutson P, Ghiani CA, Zhou JM, Gallo V, McBain CJ (1997) K^+ channel expression and cell proliferation are regulated by intracellular sodium and membrane depolarization in oligodendrocyte progenitor cells. J Neurosci 17:2669–2682.
Kohl NE, Omer CA, Conner MW, Anthony NJ, Davide JP, deSolms SJ, Giuliani EA, Gomez RP, Graham SL, Hamilton K, Handt LK, Hartman GD, Koblan KS, Kral AM, Miller PJ, Mosser SD, O'Neill TJ, Rands E, Schaber MD, Gibbs JB (1995) Inhibition of farnesyltransferase induces regression of mammary and salivary carcinomas in ras transgenic mice. Nat Med 1:792–797.
Konishi T (1989a) Voltage-dependent potassium channels in mouse Schwann cells. J Physiol (Lond) 411:115–130.
Konishi T (1989b) Voltage-dependent potassium channels in cultured mammalian Schwann cells. Brain Res 499:273–280.
Konishi T (1990) Voltage-gated potassium currents in myelinating Schwann cells in the mouse. J Physiol (Lond) 431:123–139.
Livesey FJ, O'Brien JA, Li M, Smith AG, Murphy LJ, Hunt SP (1997) A Schwann cell mitogen accompanying regeneration of motor neurons. Nature 390:614–618.
Mi H, Deerinck TJ, Ellisman MH, Schwarz TL (1995) Differential distribution of closely related potassium channels in rat Schwann cells. J Neurosci 15:3761–3774.
Nerbonne JM (2000) Molecular basis of functional voltage-gated K^+ channel diversity in the mammalian myocardium. J Physiol (Lond) 525:285–298.
Pak MD, Baker K, Covarrubias M, Butler A, Ratcliffe A, Salkoff L (1991) mShal, a subfamily of A-type K^+ channel cloned from mammalian brain. Proc Natl Acad Sci USA 88:4386–4390.
Pappas CA, Ritchie JM (1998) Effect of specific ion channel blockers on cultured Schwann cell proliferation. Glia 22:113–120.
Peretz A, Sobko A, Attali B (1999) Tyrosine kinases modulate K^+ channel gating in mouse Schwann cells. J Physiol (Lond) 519:373–384.
Po S, Roberds S, Snyders DJ, Tamkun MM, Bennett PB (1993) Heteromultimeric assembly of human potassium channels. Molecular basis of a transient outward current? Circ Res 72:1326–1336.
Rasband MN, Trimmer JS, Schwarz TL, Levinson SR, Ellisman MH, Schachner M, Shrager P (1998) Potassium channel distribution, clustering, and function in remyelinating rat axons. J Neurosci 18:36–47.
Riccardi VM (1991) Neurofibromatosis: past, present, and future. N Engl J Med 324:1283–1285.
Rosenbaum C, Kamleiter M, Grafe P, Kluwe L, Mautner V, Muller HW, Hanemann CO (2000) Enhanced proliferation and potassium conductance of Schwann cells isolated from NF2 schwannomas can be reduced by quinidine. Neurobiol Dis 4:483–491.
Ruby B (1988) Diversity and ubiquity of K channels. Neuroscience 25:729–749.
Sigworth FJ (1977) Sodium channels in nerve apparently have two conductance states. Nature 270:265–267.
Sigworth FJ (1980) The variance of sodium current fluctuations at the node of Ranvier. J Physiol (Lond) 307:97–129.
Sobko A, Peretz A, Shirihai O, Etkin S, Cherepanova V, Dagan D, Attali B (1998a) Heteromultimeric delayed-rectifier K channels in Schwann cells: developmental expression and role in cell proliferation. J Neurosci 18:10398–10408.
Sobko A, Peretz A, Attali B (1998b) Constitutive activation of delayed-rectifier potassium channels by a src family tyrosine kinase in Schwann cells. EMBO J 17:4723–4734.
Stewart HJ, Eccleston PA, Jessen KR, Mirsky R (1991) Interaction between cAMP elevation, identified growth factors, and serum components in regulating Schwann cell growth. J Neurosci Res 30:346–352.
The I, Hannigan GE, Cowley GS, Reginald S, Zhong Y, Gusella JF, Hariharan IK, Bernards A (1997) Rescue of a *Drosophila* NF1 mutant phenotype by protein kinase A. Science 276:791–794.
Tong J, Hannan F, Zhu Y, Bernards A, Zhong Y (2002) Neurofibromin regulates G protein-stimulated adenylyl cyclase activity. Nat Neurosci 5:95–96.
Tsien RW, Bean BP, Hess P, Lansman JB, Nilius B, Nowycky MC (1986) Mechanisms of calcium channel modulation by beta-adrenergic agents and dihydropyridine calcium agonists. J Mol Cell Cardiol 18:691–710.
Upadhyaya M, Shen M, Cherryson A, Farnham J, Maynard J, Huson SM, Harper PS (1992) Analysis of mutations at the neurofibromatosis 1 (NF1) locus. Hum Mol Genet 1:735–740.
Wallace MR, Marchuk DA, Andersen LB, Letcher R, Odeh HM, Saulino AM, Fountain JW, Brereton A, Nicholson J, Mitchell AL, Brownstein BH, Collins FS (1990) Type 1 neurofibromatosis gene: identification of a large transcript disrupted in three NF1 patients. Science 249:181–186.
Wilson GF, Chiu SY (1993) Mitogenic factors regulate ion channels in Schwann cells cultured from newborn rat sciatic nerve. J Physiol (Lond) 470:501–520.
Xu GF, Lin B, Tanaka K, Dunn D, Wood D, Gesteland R, White R, Weiss R, Tamanoi F (1990) The catalytic domain of the neurofibromatosis type 1 gene product stimulates ras GTPase and complements ira mutants of *S. cerevisiae.* Cell 63:835–841.
Yamoah EN (1997) Potassium currents in presynaptic hair cells of Hermissenda. Biophys J 72:193–203.
Zhong Y (1995) Mediation of PACAP-like neuropeptide transmission by coactivation of Ras/Raf and cAMP signal transduction pathways in *Drosophila*. Nature 375:588–592.